# Nanobioremediation: A Sustainable Approach for Wastewater Treatment


**Sougata Ghosh, Bishwarup Sarkar, and Sirikanjana Thongmee**

**Abstract** Urbanization and industrial revolution has led to the pollution of the existing water bodies at an alarming rate. Heavy metals, pesticides, dye, oil spills and other hazardous chemicals are among the key refractory pollutants that cannot be removed effectively by the conventional wastewater treatment processes which are often expensive and have high energy requirements. Nanotechnology is employed in various fields more recently that include textiles, food, pharmaceutics, agriculture and even environment. Small dimension of the nanoparticles offers larger surface area for adsorption of the toxic pollutants that can be eventually removed. Such nanoparticles have exotic physicochemical and optoelectronic properties that determine their appropriate field of applications. Nanotechnology driven solutions for wastewater treatment is not only rapid and efficient but also economical. In view of the background, this chapter discusses in detail, the recent advances in the field of wastewater nanobioremediation through application of various surface active nanostructures. Photocatalytic degradation of pollutants in wastewater by nanostructured catalyst in presence of appropriate source of illumination has been reported in several studies. Some of the common nanocatalysts covered here include titanium dioxide ($TiO_2$), zinc oxide (ZnO), ferric oxide ($Fe_2O_3$), zinc sulfide (ZnS), magnetic nanoparticles (MNPs). Further, pressure-driven nanofiltration using different nanomaterials such as carbon, metal oxides are also elaborated. Eventually, nanosorbents mediated removal of several organic and inorganic pollutants from wastewater samples are also covered. Hence, further optimization and scale up of nanomaterial mediated wastewater treatment can help to implement the process for treating industrial effluents to ensure a safe environment.

S. Ghosh (✉) · S. Thongmee
Faculty of Science, Department of Physics, Kasetsart University, Bangkok, Thailand
e-mail: ghoshsibb@gmail.com

S. Ghosh
Department of Microbiology, School of Science, RK. University, Rajkot, Gujarat, India

B. Sarkar
College of Science, Northeastern University, Boston, MA, USA



M. P. Shah (ed.), *Modern Approaches in Waste Bioremediation*,
https://doi.org/10.1007/978-3-031-24086-7_20

**Keywords** Wastewater treatment · Refractory pollutants · Nanotechnology · Photocatalysis · Nanofiltration · Nanosorbents

## 1 Introduction

Water is a vital part of the planet which is naturally recycled to maintain an adequate supply of clean water for human consumption (Bora and Dutta 2014). However, uncontrolled growth rate of the human population along with excessive industrialization has resulted in shortage of potable water in various parts of the world (Luikham et al. 2018). In addition, majority of water supply processes require a large amount of resources that are primarily involved in purification and treatment of wastewater to control the organic and inorganic content in such contaminated water samples (Chorawala and Mehta 2015).

Conventional wastewater treatment methods are cumbersome and typically consists of three stages namely, preliminary, primary and secondary (Ghosh 2020). Moreover, the treated samples are also subjected to ultraviolet (UV) disinfection before they could be discharged into the water bodies. In some instances, tertiary methods are also employed to remove trace amounts of contaminants which are extremely costly (Ghosh et al. 2021a, b). Hence, novel, cost-effective and improved wastewater treatment methods are required that are rapid and environment friendly as well (Qu et al. 2013). Nanotechnology has recently been demonstrated to provide such solutions wherein different nanomaterials such as titanium dioxide ($TiO_2$), zinc oxide (ZnO), polymer membranes, carbon nanotubes (CNTs), and magnetic nanoparticles (MNPs) were used for effective wastewater treatment (Ghosh and Webster 2021a, b; Ghosh et al. 2021c, d, e). Therefore, this chapter discusses in detail the use of nanomaterials for photocatalysis, nanofiltration as well as nanosorption of organic and inorganic pollutants from wastewater. Different kinds of nanomaterials are summarized in Table 1 that have effectively displayed removal of various pollutants such as dyes, heavy metals, organic and inorganic pollutants from wastewater samples. Further studies on improvements, optimization and risk evaluation of these nanomaterials for their application in the environment can provide an effective nano-based wastewater treatment method that can be useful on a large scale.

## 2 Photocatalysis

Metal and metal oxide nanoparticles with attractive physicochemical and optoelectronic properties are reported to show promising catalytic activity that can be exploited for degradation and removal of refractory pollutants (Ghosh et al. 2016a, b, c; Shende et al. 2017, 2018; Karmakar et al. 2020). In a recent study, Abd Elkodous et al. (2021) loaded carbon nanomaterials onto nanocomposite matrix that was utilized for photocatalytic treatment of wastewater. The matrix was made

**Table 1** Nanomaterials used for removal of refractory pollutants for treatment of wastewater

| Type of nanomaterial | Pollutant degraded | Maximum removal | References |
|---|---|---|---|
| *Photocatalysis* | | | |
| CNFST/C-dots 10%, CNFST/rGO 10%, and CNFST/SWCNTs 10% nanocomposites | Chloramine-T | 65% | Abd Elkodous et al. (2021) |
| SeSnNPs | Methylene blue and malachite green | 98% and > 95% | Saray et al. (2019) |
| $TiO_2$NPs | Cyanide | – | Ijadpanah-Saravy et al. (2014) |
| ZnS QDs | Naphthalene | 95% | Rajabi et al. (2016) |
| ZnSe/PANI nanocomposite | Methylene blue, Cr(VI) | >50% | Shirmardi et al. (2018) |
| *Nanofiltration* | | | |
| Cellulose acetate NF membrane | Sulphate, sodium and calcium | – | Choi et al. (2002) |
| Commercial nanofilter | Potassium, chloride | – | Nataraj et al. (2006) |
| ES10, ES10C, LES90, LF10, NTR729HF, and NTR-7410 | Various organic and inorganic pollutants | – | Thanuttamavong et al. (2002) |
| MPF34, NF90, and NF270 | Arsenite, sulphate, and chloride | 68%, 98%, and 84% | Andrade et al. (2017) |
| Polyacrylonitrile (PAN) membrane with polydopamine (PDA)/polyethyleneimine (PEI) layer and β-FeOOH nanorods | Methyl blue, Congo red, methyl orange and rhodamine B | 100%, 100%, 69.9% and 77.3% | Lv et al. (2017) |
| *Nanosorption* | | | |
| GEPCD-MNPs | Congo red and Cr(VI) | – | Cai et al. (2017a) |
| GO/Chitosan–PVA nanopolymer composite | Congo red | 88.17% | Das et al. (2020) |
| NiONPs | Rhodamine B dye | 76% | Motahari et al. (2015) |
| Polyindole nanofiber | Cu(II) | 121.95 mg | Cai et al. (2017b) |
| PVA coated PES-$TiO_2$ nanohybrid membrane | Organics, salts and ammonia–nitrogen | 95.83%, 72.40% and 95.66% | Kusworo et al. (2021) |

up of $Co_{0.5}Ni_{0.5}Fe_2O_4/SiO_2/TiO_2$ (CNFST) that was conjugated with C-dots, single walled-carbon nanotubes (SWCNTs), and graphene oxide (rGO) nanomaterials. X-ray diffraction (XRD) patterns of the nanocomposites then displayed anatase phase of the titanium dioxide ($TiO_2$) that was one of the primary components of the matrix along with presence of the three different carbon nanomaterials loaded onto the CNFST. Further, scanning electron microscopy (SEM) displayed uniform distribution of C-dots and rGO nanomaterials over the surface of CNFST while SWCNTs demonstrated sheet-like soots as well as uniform cross-linking with CNFST. Thereafter, transmission electron microscopy (TEM) results demonstrated spherical shaped particles with an average diameter of 90 ± 14 nm. Brunauer–Emmett–Teller (BET) surface area of the synthesized nanocomposites loaded with rGO and C-dots was smaller when compared to standard $TiO_2$ photocatalyst (P25) samples which was a result of increase in size of the nanoformulations as well as poor loading or increased agglomeration of the conjugated carbon nanomaterials. On the other hand, SWCNTs conjugation led to significant increase in the surface area. The pores in all the conjugated samples were multimodal and broad-shaped wherein the mesopores had a diameter ranging from 2 to 50 nm while the macropores had a diameter greater than 50 nm. Raman analysis further showed anatase $TiO_2$ as the dominant phase in the nanomaterial coated nanomatrix.

A comparative study of the three different carbon-loaded nanocomposites showed 28, 32.7, and 41.6% chloramine-T dye degradation by the CNFST/C-dots 10%, CNFST/rGO 10%, and CNFST/SWCNTs 10% nanocomposites, respectively after 40 min of ultraviolet (UV) irradiation. Moreover, subsequent increase in contact time to 90 min resulted in further increase in dye degradation ability with best removal activity observed using CNFST/SWCNTs 10% nanocomposites. In addition, the increase in the dosage concentration of the prepared nanoformulations resulted in subsequent increase in photocatalytic degradation of dye. Likewise, dye degradation ability of the CNFST/SWCNTs 10% nanocomposites was increased from 35 to 65% with concomitant decrease in the pH value of the system from 10.0 to 3.0, respectively. The zeta potential of the SWCNTs loaded nanocomposite was +15 mV which facilitated effective binding of the dye through electrostatic attraction for improved photocatalytic activity. The primary reactive oxygen species (ROS) mediated chloramine-T dye degradation was mainly attributed to the hydroxyl radical that was further scavenged on addition of isopropanol resulting in 40% decrease in dye degradation.

Organic pollutants were also reported to be degraded by tin selenide nanoparticles (SnSeNPs) that were prepared using co-precipitation method (Saray et al. 2019). XRD pattern analysis demonstrated orthorhombic phase of the particles. However, the crystallinity of the particles was dependent upon the Se/Sn ratio wherein a ratio of 1.0 resulted in formation of crystalline particles while particles made with a Se/Sn ratio of 1.3 did not exhibited a crystalline phase. Moreover, field emission scanning electron microscopy (FESEM) and TEM results demonstrated complete agglomeration of the particles when the Se/Sn ratio was 0.8 with presence of oxygen as impurity as confirmed by energy dispersive X-ray (EDX) spectroscopy results. Meanwhile, particles with Se/Sn ratio of 1.2 were pure and smaller in size. The photocatalytic

activity of the prepared SnSeNPs was then evaluated in which methylene blue degradation was analysed in presence of visible light. NPs prepared using a Se/Sn ratio of 1.2 was able to effectively degrade 98% of methylene blue dye within 25 min of incubation. Furthermore, the reusability of the nanomaterials was also evaluated wherein similar dye reduction ability of the SnSeNPs was observed after four successive cycles. The phase of the NPs prepared using Se/Sn ratio of 1.2 was stable as observed in XRD patterns even after four cycles of dye degradation while particles with Se/Sn ratio of 0.8 completely changed its phase after four successive photocatalytic processes. Likewise, malachite green degradation ability was also monitored in presence of the SnSeNPs with varying ratios of Se and Sn, respectively. More than 95% of the dye was effectively degraded by NPs with Se/Sn ratio of 1.0 within 45 min of incubation. The textural properties of the NPs were also evaluated wherein a maximum specific surface area equivalent to 77.441 $m^2/g$ was observed with Se/Sn ratio of 1.2 along with a pore diameter and volume of 2.43 nm and 0.124 $cm^3/g$, respectively. The energy of the valence bond of SnSeNPs with Se/Sn ratio of 1.2 was calculated to be 1.21 eV that was further used for investigating the electronic structure of the particles. Therefore on the basis of electronic structure, formation of hydroxyl radical using SeSnNPs was proposed to facilitate efficient dye degradation which could be applicable in wastewater treatment as well.

In another study, Ijadpanah-Saravy et al. (2014) reported fabrication of titanium dioxide nanoparticles ($TiO_2$NPs) by controlled hydrolysis of 3 M titanium tetrachloride. The nanomaterial demonstrated photocatalytic degradation of cyanide in wastewater samples. X-ray diffraction (XRD) patterns then displayed characteristic peaks of anatase and rutile form of $TiO_2$NPs with a crystalline size of 18 and 22 nm, respectively while scanning electron microscopic (SEM) images demonstrated spherical morphology of the particles with an average size of 20 nm. Thereafter, the photocatalytic properties of the NPs were determined wherein a 4:1 ratio of anatase to rutile form of the particles was optimal for maximum photocatalytic activity to degrade cyanide. Interestingly, pH 11 was optimal for cyanide degradation with maximum photocatalytic efficiency as well as lowest electrical energy consumption as compared to other catalysts.

Rajabi et al. (2016) also demonstrated effective photocatalytic removal of industrial pollutants using zinc sulphide quantum dots (ZnS QDs). Fast and efficient chemical precipitation technique was followed for preparation of ZnS QDs which exhibited a blue shift in UV–vis absorption peak at 235 nm that was attributed to the particle size decrease, band-gap energy increase as well as due to quantum size confinement effect. Additionally, the direct optical band gap value of the prepared nanomaterial was 4.09 eV. XRD patterns then demonstrated a cubic zinc blend crystalline structure of the ZnS QDs without presence of any impurities. TEM image analysis further revealed spherical shape of the QDs with an average dimension of around 1 nm. Thereafter, naphthalene was used for demonstrating pollutant degradation activity of the prepared ZnS QDs wherein only 25–31% degradation was obtained in absence of light. An optimal pH of 11 resulted in maximum degradation efficiency of naphthalene which was decreased with concomitant increase in initial concentration of the pollutant. Moreover, a rapid increase in degradation rate was observed for

90 min that was reduced for the next 45 min followed by equilibrium. A low initial concentration of 10 mg of ZnS QDs then demonstrated up to 95% naphthalene degradation efficiency that remained fairly constant up to four cycles highlighting its reusability. Further, a maximum degradation rate constant of $6.90 \times 10^{-5}$ $min^{-1}$ was attained when the initial concentration of naphthalene was 20 ppm. The mechanism of degradation was then proposed to involve photoexcitation that may have resulted in electron–hole pair formation on the surface of ZnS QDs semiconductor that may have then oxidized naphthalene to 2-formylcinnamaldehyde.

Shirmardi et al. (2018) also demonstrated improved photocatalytic activity of zinc selenide nanoparticles (ZnSeNPs) after addition of polyaniline (PANI) that acted as an organic semiconductor. The ZnSe/PANI nanocomposite was prepared using co-precipitation technique whose heterostructure form was confirmed by XRD patterns. In addition, TEM images showed a distinct ZnSeNPs core and PANI shell structure whereas high resolution transmission electron microscopy (HRTEM) images demonstrated interplanar distance of 0.33 nm between the zinc blend structure as evident from Fig. 1. Raman spectroscopy of the nanocomposite indicated a weaker ZnSe peak at 500 $cm^{-1}$ as compared to pristine ZnSeNPs that was attributed to the presence of PANI shell in the composite. Raman spectrum of the nanocomposite also demonstrated two other peaks at 1105 and 420 $cm^{-1}$ that corresponded with C-H vibration of the semi-quinonoid rings and out-of-plane ring-deformation of PANI, respectively. X-ray photon spectroscopy (XPS) based valence band (VB) spectral analysis then demonstrated a nanocomposite VB potential of $0.48 \pm 0.05$ eV while the pristine ZnSeNPs had a VB potential of approximately 1.13 eV. Further, methylene blue dye degradation ability of the prepared nanocomposite was analysed under visible light irradiation. More than 50% of the initial dye concentration was reduced by the ZnSe/PANI nanocomposite within 30 min whereas it took 120 min for the pristine ZnSeNPs for completing similar levels of reduction. Additionally, presence of PANI displayed an increase in photocurrent intensity along with a decrease in the photoconductivity resistance. In addition, ZnSe/PANI nanocomposite was also investigated for its inorganic pollutant removal activity wherein absorption peak of $K_2Cr_2O_7$ at 375 nm was decreased in presence of the nanocomposite with gradual increase in visible light irradiation time. Hence, Cr(VI) ions were reduced to Cr(III) efficiently by the nanocomposite as well.

## 3 Nanofiltration

Nanoparticles impregnated polymeric films are often used as superior membranes for nanofiltration of water in order to remove certain hazardous pollutants which are recalcitrant in nature (Ghosh et al. 2022a, b; Ghosh and Webster 2022). Nataraj et al. (2006) removed colour and contaminants from distillery effluent using a hybrid system of nanofiltration (NF) combined with reverse osmosis (RO). A commercial nanofilter as well as thin-film composite (TFC) polyamide RO membrane was used in this study wherein effective colour removal ability of the NF was attained when

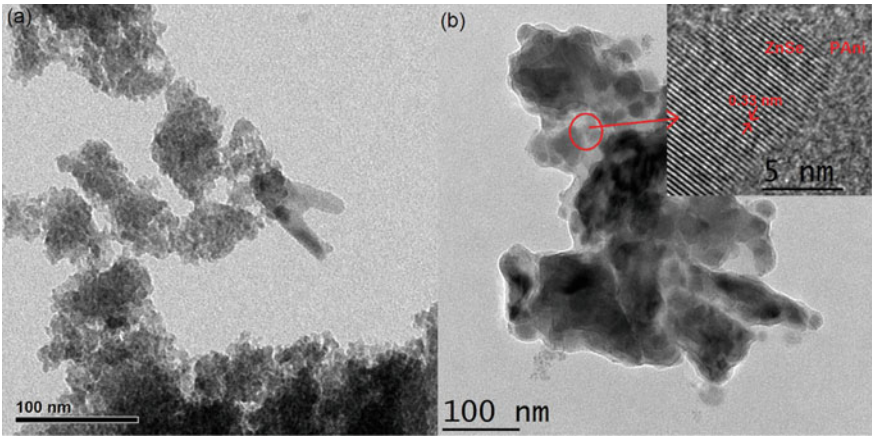


**Fig. 1** TEM image of **a** pristine ZnSe NPs and **b** ZnSe/PANI nanocomposites. The inset shows an HRTEM image of ZnSe/PANI nanocomposites. Reprinted from Shirmardi A, Teridi MA, Azimi HR, Basirun WJ, Jamali-Sheini F, Yousefi R, 2018. Enhanced photocatalytic performance of ZnSe/PANI nanocomposites for degradation of organic and inorganic pollutants. Applied Surface Science 462:730–738. Copyright © 2018 Elsevier B.V

the size of the particles was in the colloidal range. Thus, in at an optimal pressure of 30–50 bar, the total dissolved solids (TDS) was reduced from 51,500 to 9050 ppm while conductivity and chloride concentration was reduced from 346 mS/cm and 4900 ppm to 15.06 mS/cm and 2650 ppm, respectively. High rejection efficiency against bivalent and trivalent ions was also exhibited by the NF membrane. Thereafter, evaluation of RO based pollutant removal was performed. The impact of feed pressure on the permeate properties was analysed in which the pressure increased linearly from 20 to 70 bar when distillery spent wash was used as feed. TDS and chemical oxygen demand (COD) rejection was altered from 83 to 99.06% and 95.6 to 98.96%, respectively when 50 bar pressure was applied. Additionally, high rejection percentages for potassium and chloride ions were observed.

Choi et al. (2002) used a cellulose acetate NF membrane for treatment of wastewater. The effective surface area of the hollow NF membrane used in this study was 11.7 $m^2$ along with 55% salt rejection property. A membrane bioreactor (MBR) system was set up to evaluate the efficacy of treatment which was operated for 71 days. The transmembrane pressure along with the relative productivity permeate after 20 days of incubation were 36 kPa and 1.0–1.2, respectively after which a drastic increase in relative productivity was observed. The change in sulphate, sodium and calcium ions concentration were similar to that of conductivity wherein no electrolytes were accumulated in the bioreactor due to charge effect of the membrane. It was hence proposed that the bioreactor could be operated under low suction pressure as the effect of osmotic pressure was insignificant along with high rejection of organic matter. The biodegradable membrane remained stable for 60 days in the bioreactor wherein nitrification and denitrification occurred simultaneously. In addition, atomic

force microscope (AFM) images revealed a larger surface roughness on the cellulose acetate membrane after 40 days of bioreactor operation which was further increased till 71 days thus highlighting biodegradation of the membrane.

Thanuttamavong et al. (2002) also characterized NF rejection efficiency of organic and inorganic pollutants for treatment of wastewater. Six different commercial NF membranes namely ES10, ES10C, LES90, LF10, NTR729HF, and NTR-7410 were used in this study that were composed of aromatic polyamides, polyvinyl alcohols, and sulfonated polysulfones. The total dissolved organic and inorganic content of the polluted water sample were 1.8 mg/L and 3 mM, respectively. The pH and the turbidity of the water samples were in the range of 7.2–7.5 and 2.5–5.5 NTU, respectively. Long-term operations for a time period of 120 and 20 days were carried out with and without microfiltration pre-treatment, respectively. A transmembrane pressure of 0.15 MPa was maintained in both cases along with a standardized permeate flux temperature of 25 °C. A significant decline in permeate flux was observed for all the membranes during the first 10 days of operation. The permeate flux of the untreated loose membrane NTR7410 continuously declined and reached a steady state value of 0.28 m/d in 15 days of operation whereas the treated membranes showed a faster steady state attainment. Further, a stable rejection of all the components was observed throughout the NF operation which highlighted that membrane fouling does not interfere with the rejection mechanisms. Additionally, significant change in zeta potential values of the membrane surface was observed after long-term operation. The MWCO value for ES-10, ES-10C, LES-90 and LF-10 was 100 Da while it was 200 Da and more than 350 Da for NTR-729HF and NTR-7410, respectively. Moreover, organic matter with a size range of 300–1800 Da was found in the permeate of NTR7410 NF membrane. With regards to inorganic matter rejection, divalent ions such as $Ca^{2+}$ and $Mg^{2+}$ exhibited higher rejection as compared to monovalent ions such as $Na^{+}$ and $Cl^{-}$ which was attributed to the charge effect of the membrane. Thereafter, the effective charge density of the NTR-729HF membrane was changed from $-2$ to $-0.5$ mol/L after long-term operation which suggested a decrease in the electrostatic property of the membrane after its utilization. The partitioning coefficient of the membrane for nitrate ion was also decreased from 5.0 to 2.6 after operation.

Likewise, Andrade et al. (2017) demonstrated gold mining effluent treatment using NF and compared with RO. Five different membranes were used in this study namely, TFC-HR and BW30 that were RO membranes while MPF34, NF90, and NF270 were the three NF membranes. The permeate flux of RO membranes were 7–12 folds lower than NF membranes that was attributed to higher resistance in the RO membrane. Moreover, a more intense membrane fouling was also observed in case of TFC-HR whereas MPF34 exhibited minimum fouling. The initial pollutant retention efficiency of all the membranes was considerably high. However, a high sulphate concentration in the mining effluent was proposed to interfere with the reuse of water as it could cause metal precipitation which could further result in membrane fouling. Among the RO membranes, TFC-HR demonstrated maximum pollutant retention efficiency with 75%, 99%, and 78% retention of arsenic, sulphate, and chloride ions, respectively. Similarly, NF90 membrane exhibited excellent arsenic,

sulphate, and chloride retention of 68%, 98%, and 84%, respectively. Moreover, the effluent was pre-treated to increase its pH which resulted in decrease in conductivity as well as concentrations of calcium and magnesium. Concentration of arsenic was also reduced with subsequent increase in pH of the effluent from 2.2 to 5.0 that subsequently enhanced recovery rate from 27 to 70% along with higher resistance to membrane fouling. The permeate recovery rate (RR) was also studied in which the quality of the permeate remained almost similar when the RR value was up to 40% above which the removal efficiency started to gradually decrease. The concentration of polarization of NF membranes was then increased to 1.45 using a synthetic solution of $MgSO_4$ which resulted in increase of RR to 70% while decreasing the removal efficiency. Hence, it was concluded that such NF based effluent treatment could be optimal as well as feasible for obtaining industrial water samples from the same.

Lv et al. (2017) reported fabrication of a photocatalytic nanofiltration (NF) membrane that had self-cleaning property and thus, could be used for wastewater treatment as represented schematically in Fig. 2. Co-deposition method was carried out on an ultrafiltration polyacrylonitrile (PAN) membrane with polydopamine (PDA)/polyethyleneimine (PEI) to form an intermediate layer after which β-FeOOH nanorods were mineralized to further create a photocatalytic layer on the NF system. X-ray photoelectron spectrometer (XPS) results of the mineralized membrane then displayed additional binding energy peaks at Fe 2p along with a change in oxygen/carbon ratio from 0.32 to 1.22 which confirmed presence of FeOOH group on the membrane surface. SEM images also demonstrated uniform distribution of β-FeOOH nanorods over the surface of the membrane with a vertical orientation and a thickness of around 0.45 μm. The enhanced wettability of the membrane was analysed through calculation of the dynamic water contact angle that was decreased from 60° to 20° within 100 s. Such improved permeability of the mineralized membrane was attributed to the hydrophilicity of the β-FeOOH nanorods that were attached on the surface of the membrane. The surface charge properties of the membrane were then analysed wherein the isoelectric point of the membrane surface decreased from 6.3 to 5.6 after mineralization. In addition, the molecular weight cut-off (MWCO) value showed a steady decrease from 20,000 to 2000 Da with subsequent increase in deposition time from 1 to 6 h, respectively. Thereafter, the dye rejection performance of the stable mineralized NF membrane was studied in which 100% rejection of methyl blue and Congo red was attained at pH 3 and 7, respectively with a deposition time of 2 h. Likewise, 60.8 and 69.9% of methyl orange rejections were observed at pH 7 and 3, respectively. On the other hand, rhodamine B dye rejection was increased up to 77.3% when a positive surface charge was attained on the membrane. Thereafter, a continuous cross-flow membrane reactor was set up for observing the photocatalytic performance of the prepared membranes. The colour of the feed solution containing 20 mg/L of methyl blue and 30% $H_2O_2$ became colourless after 6 h of incubation. The self-cleaning property of the membrane was also evaluated by immersing the fouling membrane into an acidic $H_2O_2$ solution and in presence of visible light wherein the water flux was recovered to its original value. A high NF performance of 97.3% was achieved even after five successful photocatalytic cycles indicating its reusability and recyclability.

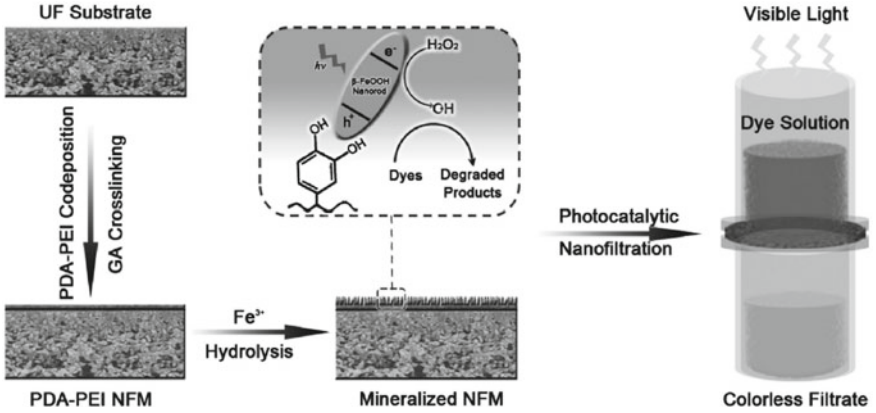


**Fig. 2** Schematic representation of preparation process for the β–FeOOH mineralized NFM and its application in photocatalytic nanofiltration. Reprinted with permission from Lv Y, Zhang C, He A, Yang SJ, Wu GP, Darling SB, Xu ZK, 2017. Photocatalytic nanofiltration membranes with self-cleaning property for wastewater treatment. Advanced Functional Materials 27:1,700,251. Copyright © 2017 WILEY–VCH Verlag GmbH & Co. KGaA, Weinheim

## 4 Nanosorption

Nanocomposite based adsorbents are advantageous compared to conventional sorbents due to their superior ability for purification and convenience in manipulation of their activity by rational physico-chemical modification. Cai et al. (2017a) also reported formulation of a novel multi-layer magnetic adsorbent (GEPCD-MNPs) using ring opening polymerization process wherein a multi-layer cationic polymer was coated on the surface of magnetic nanoparticles (MNPs). These nano-adsorbents were then utilized for dyeing wastewater treatment. SEM images of the nano-adsorbents showed spherical morphology of the MNPs that had a smaller diameter as compared to pristine MNPs which suggested presence of the polymer on the active sites of MNPs. The contact angle of the nano-adsorbent was less than 90° when immersed in Congo red and Cr(VI) containing solutions thus indicating its hydrophilicity. The magnetic properties of the nano-adsorbent were also evaluated which provided a saturation magnetization value of 54.7 emu/g. The removal efficiency of Congo red increased with subsequent increase in the pH value of the system from 7.25 to 9.25 that was attributed to protonation of the MNPs and the functional groups of the polymer which may result in improved coordinate affinity with the dye. On the contrary, removal rate of Cr(VI) from the solution decreased with concomitant increase in pH value from 2.98 to 11.94 which was proposed to transform $Cr_2O_7^{2-}$ into $CrO_2^-$ that has lower electrostatic interaction with the nano-adsorbent. The adsorption kinetics analyses for Congo red and Cr(VI) adsorption followed a pseudo-second order reaction while both the Langmuir and Freundlich adsorption isotherm models were properly fitted for the adsorption processes. Therefore, GEPCD-MNPs

were proposed to be economically viable and effective nano-adsorbents that could be potentially be used in large-scale wastewater treatment processes with further optimization.

A hybrid hydrogel nanopolymer was prepared by Das et al. (2020) using graphene oxide (GO), chitosan and polyvinyl alcohol (PVA) that was investigated for its wastewater treatment efficacy. SEM images of the prepared GO reinforced chitosan-PVA hydrogel nanopolymer displayed homogenous distribution of GO over the matrix without any agglomeration. Fourier transform infrared (FTIR) spectroscopy analysis then displayed peaks at 3268.06 and 1377.33 $cm^{-1}$ which corresponded with $–NH_2$ stretching vibrations of chitosan and $–CH_2$ deformation vibrations of PVA due to cross-linking, respectively. FTIR spectra of the prepared nanopolymer then displayed characteristic peaks corresponding with surface functional groups of chitosan, PVA and GO. A maximum positive surface charge on the nanopolymer membrane was observed at a pH value of 3.3 that was considered ideal for anionic dye adsorption. The swelling behaviour of the nanopolymer membrane was also evaluated wherein maximum swelling of 17.24 g/g was achieved after 90 min of immersion in water that further increased to 25.89 g/g at a pH value of 2.0. This change was attributed to ionization of the functional groups present on the membrane. Thereafter, dye adsorption studies were conducted using a biological oxygen demand (BOD) shaker at 140 rotations per minute (rpm) under room temperature. A maximum Congo red dye removal efficiency of 84.31% was obtained at an initial dye concentration of 10 mg/L. Additionally, the adsorption efficiency increased from 76.62 to 81.1% with subsequent increase in dosage of adsorbent from 1 to 6 g/L, respectively. An acidic pH of 2.0 was further demonstrated to provide maximum adsorption efficiency of 88.17% because of effective electrostatic interaction between the cationic nanopolymer membrane and anionic dye molecules. Adsorption isotherm studies predicted that Langmuir model was best fitted for explaining the dye adsorption while adsorption kinetics revealed pseudo second order reaction of the adsorption process.

In another study, Motahari et al. (2015) cost-effectively synthesized nickel oxide nanoparticles (NiONPs) for rhodamine B dye removal from wastewater samples. $H_2$acacen ligand was used for hydrothermal formation of nano-scale $Ni(OH)_2$ followed by calcination to obtain NiONPs. XRD patterns of the prepared NPs corresponded with the face-centered cubic as well as crystalline structure of nickel oxide. FESEM images then displayed monodispersed NiONPs while TEM micrographs showed spherical morphology of the particles with an average size of 10 nm. The BET surface area of the NiONPs was 176.56 $m^2/g$ that were porous in nature with an average pore size of around 9.7 nm. Later on, dye adsorption studies were carried out in which 76% of rhodamine B dye at a concentration of 10 mg/L was efficiently removed within the initial 30 min of reaction. The reusability of the particles was also highlighted wherein no change in dye adsorption activity was observed after reusing the same particles. Adsorption isotherm studies then provided maximum dye adsorption capacity of 111 mg/g using Langmuir isotherm model whereas kinetic studies showed suitability of pseudo second order reaction for explaining the NiONPs

mediated rhodamine B dye adsorption reaction. Optimal pH 7.0 then demonstrated efficient dye adsorption that was exothermic in nature as the dye adsorption capacity decreased with subsequent increase in the temperature of the system.

Cai et al. (2017b) also fabricated polyindole nanofibers using electrospinning that could act as nano-adsorbent for removal of heavy metal ions from wastewater. SEM and TEM images displayed spherical morphology of the nanofibers that had a smooth surface along with an average diameter range of 140–300 nm. The ranges of pore size, diameter and specific surface area were 0.217–0.250 $cm^3\ g^{-1}$, 55–68 nm and 64.43–86.41 $m^2\ g^{-1}$, respectively. Moreover, the specific surface area and pore volume decreased with concomitant decrease in the fibre diameter while the opposite was observed for the pore diameter. Thereafter, effect of pH on the metal adsorption capacity of the nanofibers was investigated wherein maximum Cu(II) adsorption was observed at an acidic pH value of 6.0 that was used for further experiments in this study. The maximum adsorption capacity of the nanofibers having a polyindole concentration of 1.6% was 121.95 mg/g within 15 min of incubation that was the most effective contact time as well. In addition, the Cu(II) adsorption capacity of the nanofiber was insignificantly affected in presence of low concentrations of other metal ions such as $Na^+$, $K^+$, $Mg^{2+}$ and $Ca^{2+}$ that highlighted the specific Cu(II) adsorption capacity of the nanofibers. Moreover, the adsorption isotherm studies then demonstrated Langmuir model to be a best fit for the Cu(II) adsorption using polyindole nanofibers. Additionally, the pseudo second order reaction was followed by the adsorption process. Moreover, the reusability of the nanofiber was also investigated wherein the adsorption efficiencies were 95%, 88.7% and 82% of the original adsorption capacity of the nanofibers after the third, fifth and seventh cycle, respectively. In addition, Cu(II) adsorption by the nanofibers was proposed to be mediated by chemisorption which consists of coordination between the metal ion and nitrogen containing functional groups of the membrane may result in chelation.

In another similar study, a nanohybrid membrane that was cross-linked with PVA and coated with polyether sulfone (PES)-$TiO_2$NPs was reported as an effective adsorbent in wastewater treatment (Kusworo et al. 2021). SEM images of the prepared membranes showed a smooth surface with minimal nodules while the sub-layer structures of the membrane were asymmetric with a dense skin layer along with a porous sub-layer made up of finger-like structures as evident from Fig. 3. XRD patterns of PVA coated PES-$TiO_2$ nanohybrid membrane further showed a wide band at 19–20° that corresponded with orthorhombic lattice along with the polycrystalline behaviour of PVA along with weak bands that highlighted the amorphous PES and $TiO_2$ crystalline peaks. In addition, the water contact angle of the 3.0 wt.% PVA complexed nanohybrid membrane was 27.67° that highlighted its hydrophilicity. Mechanical properties of the 3.0 wt.% PVA linked membrane was also studied that demonstrated a thickness of 90 μm with a tensile strength and elongation break of $6.4 \pm 0.15$ MPa and $1.6 \pm 0.10$%, respectively. Thereafter, addition of $TiO_2$NPs on the membrane was attributed to the increase and stabilization of the permeate flux at 80 $L/m^2/h$ as it could degrade the attached foulants. Hence, gradual increase in $TiO_2$ concentration resulted in improved COD, total dissolved solids (TDS), surface wettability as well as rejection percentages. Likewise, addition of PVA resulted in considerable increase

in COD, TDS, and $NH_3$-N rejection by 244.80%, 56.70%, and 5.29%, respectively. Furthermore, organics, salts and ammonia–nitrogen rejection were also enhanced up to 75.00%, 51.61%, and 90.47% that was further improved by 95.83%, 72.40% and 95.66%, respectively when integrated with ozonation.

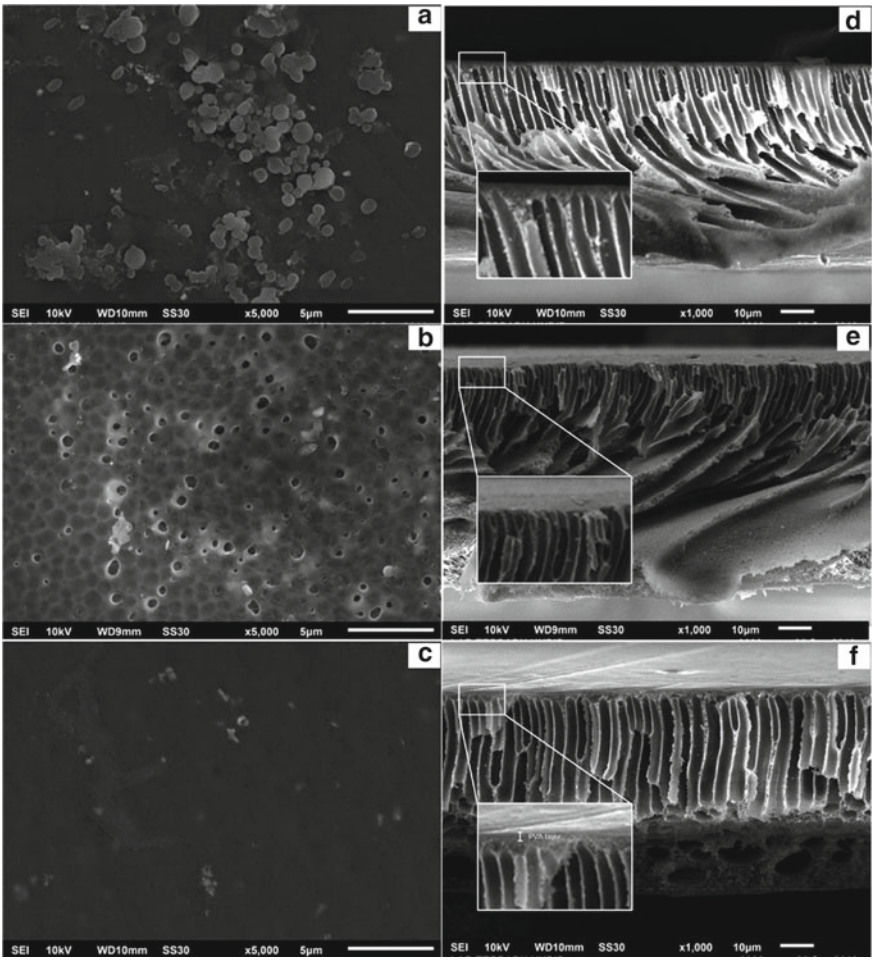


**Fig. 3** Membrane surface morphology of **a** PES-$TiO_2$ 1 wt-%, **b** PES-$TiO_2$/PVA 0.5 wt-%, **c** PES-$TiO_2$/PVA 3.0 wt-% and cross-section images of **d** PES-$TiO_2$ 1 wt-%, **e** PES-$TiO_2$/PVA 0.5 wt-%, **f** PES-$TiO_2$/PVA 3.0 wt-%. Reprinted with permission from Kusworo TD, Kumoro AC, Utomo DP, Kusumah FM, Pratiwi MD, 2021. Performance of the crosslinked PVA coated PES-$TiO_2$ nano hybrid membrane for the treatment of pretreated natural rubber wastewater involving sequential adsorption–ozonation processes. Journal of Environmental Chemical Engineering 9:104,855. 

## 5 Conclusion and Future Perspectives

Surface active nanoparticles exhibit notable physical and chemical properties that are exploited in various biomedical applications (Ghosh et al. 2018). The attractive features of the nanoparticles have extended their applications for infection control, agriculture, textiles, and even environment (Adersh et al. 2015; Rokade et al. 2017; Jamdade et al. 2019; Bhagwat et al. 2018; Ghosh et al. 2016d). The nanostructures used so far for the treatment of wastewater for photocatalysis, nanofiltration or nanosorption are either fabricated by physical or chemical methods which often use hazardous chemicals and reaction conditions (Bloch et al. 2021; Ranpariya et al. 2021). However, biological route for synthesis of metal and metal oxide nanoparticles are environmentally benign, rapid and efficient (Shinde et al. 2018). Microbe synthesized nanoparticles are reported to have efficient photocatalytic activity that can be further integrated in the membranes for effective dye degradation and removal (Ghosh 2018). Similarly, various medicinal plants like *Gloriosa superba, Dioscorea bulbifera, Gnidia glauca, Plumbago zeylanica,* and others are reported to synthesize exotic gold, silver, copper, platinum, and palladium nanoparticles that can be further explored for wastewater treatment (Rokade et al. 2018; Ghosh et al. 2015a, b, c; Jamdade et al. 2019; Salunke et al. 2014). Composite nanoparticles either bimetallic or functionalized with metal removing or dye degrading enzymes, bioactive principles can be employed for multimodal wastewater treatment (Robkhob et al. 2020; Ghosh et al. 2015d; Kitture et al. 2015). In view of the background it can be concluded that development of nanotechnology assisted strategies for wastewater treatment can serve as a powerful tool to ensure clean environment.

**Acknowledgements** Dr. Sougata Ghosh acknowledges Kasetsart University, Bangkok, Thailand for Post Doctoral Fellowship and funding under Reinventing University Program (Ref. No. 6501.0207/10870 dated 9th November, 2021 and Ref. No. 6501.0207/9219 dated 14th September, 2022).

## References

Abd Elkodous M, El-Sayyad GS, Maksoud MA, Kumar R, Maegawa K, Kawamura G, Tan WK, Matsuda A (2021) Nanocomposite matrix conjugated with carbon nanomaterials for photocatalytic wastewater treatment. J Hazard Mater 410:124657

Adersh A, Ghosh S, More PA, Chopade BA, Gandhi MN, Kulkarni AR (2015) Surface defect rich ZnO quantum dots as antioxidants inhibiting α-amylase and α-glucosidase: a potential antidiabetic nanomedicine. J Mater Chem B 3:4597–4606

Andrade LH, Aguiar AO, Pires WL, Miranda GA, Teixeira LP, Almeida GC, Amaral MC (2017) Nanofiltration and reverse osmosis applied to gold mining effluent treatment and reuse. Braz J Chem Eng 34(1):93–107

Bhagwat TR, Joshi KA, Parihar VS, Asok A, Bellare J, Ghosh S (2018) Biogenic copper nanoparticles from medicinal plants as novel antidiabetic nanomedicine. World J Pharm Res 7(4):183–196

Bloch K, Pardesi K, Satriano C, Ghosh S (2021) Bacteriogenic platinum nanoparticles for application in nanomedicine. Front Chem 9:624344

Bora T, Dutta J (2014) Applications of nanotechnology in wastewater treatment—a review. J Nanosci Nanotechnol 14:613–626

Cai D, Zhang T, Zhang F, Luo X (2017a) Quaternary ammonium β-cyclodextrin-conjugated magnetic nanoparticles as nano-adsorbents for the treatment of dyeing wastewater: synthesis and adsorption studies. J Environ Chem Eng 5:2869–2878

Cai Z, Song X, Zhang Q, Zhai T (2017b) Electrospun polyindole nanofibers as a nano-adsorbent for heavy metal ions adsorption for wastewater treatment. Fibers Polym 18(3):502–513

Choi JH, Dockko S, Fukushi K, Yamamoto K (2002) A novel application of a submerged nanofiltration membrane bioreactor (NF MBR) for wastewater treatment. Desalination 146:413–420

Chorawala KK, Mehta MJ (2015) Applications of nanotechnology in wastewater treatment. Int J Innov Emerg Res Eng 2(1):21–26

Das L, Das P, Bhowal A, Bhattachariee C (2020) Synthesis of hybrid hydrogel nano-polymer composite using graphene oxide, chitosan and PVA and its application in waste water treatment. Environ Technol Innov 18:100664

Ghosh S (2018) Copper and palladium nanostructures: A bacteriogenic approach. Appl Microbiol Biotechnol 101(18):7693–7701

Ghosh S, Nitnavare R, Dewle A, Tomar GB, Chippalkatti R, More P, Kitture R, Kale S, Bellare J, Chopade BA (2015) Novel platinum-palladium bimetallic nanoparticles synthesized by *Dioscorea bulbifera*: Anticancer and antioxidant activities. Int J Nanomed 10(1):7477–7490

Ghosh S, Jagtap S, More P, Shete UJ, Maheshwari NO, Rao SJ, Kitture R, Kale S, Bellare J, Patil S, Pal JK (2015) *Dioscorea bulbifera* mediated synthesis of novel $Au_{core}Ag_{shell}$ nanoparticles with potent antibiofilm and antileishmanial activity. J Nanomater 2015:562938

Ghosh S, More P, Nitnavare R, Jagtap S, Chippalkatti R, Derle A, Kitture R, Asok A, Kale S, Singh S, Shaikh ML, Ramanamurthy B, Bellare J, Chopade BA (2015) Antidiabetic and antioxidant properties of copper nanoparticles synthesized by medicinal plant *Dioscorea bulbifera*. J Nanomed Nanotechnol S6:007

Ghosh S, More P, Derle A, Kitture R, Kale T, Gorain M, Avasthi A, Markad P, Kundu GC, Kale S, Dhavale DD, Bellare J, Chopade BA (2015) Diosgenin functionalized iron oxide nanoparticles as novel nanomaterial against breast cancer. J Nanosci Nanotechnol 15(12):9464–9472

Ghosh S, Chacko MJ, Harke AN, Gurav SP, Joshi KA, Dhepe A, Kulkarni AS, Shinde VS, Parihar VS, Asok A, Banerjee K, Bellare J, Chopade BA (2016a) *Barleria prionitis* leaf mediated synthesis of silver and gold nanocatalysts. J Nanomed Nanotechnol 7:4

Ghosh S, Gurav SP, Harke AN, Chacko MJ, Joshi KA, Dhepe A, Charolkar C, Shinde VS, Kitture R, Parihar VS, Banerjee K, Kamble N, Bellare J, Chopade BA (2016b) *Dioscorea oppositifolia* mediated synthesis of gold and silver nanoparticles with catalytic activity. J Nanomed Nanotechnol 7:5

Ghosh S, Patil S, Chopade NB, Luikham S, Kitture R, Gurav DD, Patil AB, Phadatare SD, Sontakke V, Kale S, Shinde V, Bellare J, Chopade BA (2016c) *Gnidia glauca* leaf and stem extract mediated synthesis of gold nanocatalysts with free radical scavenging potential. J Nanomed Nanotechnol 7:358

Ghosh S, Harke AN, Chacko MJ, Gurav SP, Joshi KA, Dhepe A, Dewle A, Tomar GB, Kitture R, Parihar VS, Banerjee K (2016d) *Gloriosa superba* mediated synthesis of silver and gold nanoparticles for anticancer applications. J Nanomed Nanotechnol 7(4)

Ghosh S, Webster TJ (2021a) Nanotechnology for water processing. In: Shah MP, Rodriguez-Couto S, Mehta K (eds) The future of effluent treatment plants-biological treatment systems. Elsevier, pp 335–360. Paperback ISBN: 9780128229569

Ghosh S, Webster TJ, 2021b. Biologically synthesized nanoparticles for dye removal. In: Shah M, Couto SR, Biswas JK (eds) Removal of emerging contaminants from wastewater through bio-nanotechnology. Elsevier, pp 573–603. Paperback ISBN: 9780323855839

Ghosh S, Webster TJ (2022) Nanotechnological advances for oil spill management: removal, recovery and remediation. In: Das P, Manna S, Pandey JK (eds) Advances in oil-water separation:

a complete guide for physical, chemical, and biochemical processes. Elsevier, pp 175–194. ISBN: 978-0-323-89978-9

Ghosh S, Sanghavi S, Sancheti P (2018) Metallic biomaterial for bone support and replacement. In: Balakrishnan, P, Sreekala MS, Thomas S (eds), Fundamental biomaterials: metals, vol 2. Woodhead Publishing Series in Biomaterials, Woodhead Publishing, pp 139–165. ISBN: 0081022069 (print); ISBN: 978-0-08-102206-1 (online)

Ghosh S, Selvakumar G, Ajilda AAK, Webster TJ (2021a) Microbial biosorbents for heavy metal removal. In: Shah MP, Couto SR, Rudra VK (eds) New trends in removal of heavy metals from industrial wastewater. Elsevier B.V., Amsterdam, Netherlands, pp 213–262. eBook ISBN: 978-0-12-823108-1; Paperback ISBN: 978-0-12-822965-1

Ghosh S, Sharma I, Nath S, Webster TJ (2021b) Bioremediation-the natural solution. In: Shah MP, Couto SR (eds) Microbial ecology of waste water treatment plants (WWTPs). Elsevier, pp 11–40. eBook ISBN: 978-0-12-822504-2; Paperback ISBN: 978-0-12-822503-5

Ghosh S, Joshi K, Webster TJ (2021c) Removal of heavy metals by microbial communities. In: Shah MP, Couto SR (eds) Waste water treatment reactors: microbial community structure. Elsevier, pp 537–566. eBook ISBN: 978-0-12-824244-5; Paperback ISBN: 978-0-12-823991-9

Ghosh S, Bhagwat T, Webster TJ (2021d) Arsenic removal using nanotechnology. In: Kalamdhad A, Haq I (eds) Emerging treatment technologies for waste management. Springer Nature, Singapore, pp 73–102. eBook ISBN: 9789811620157; Paperback ISBN: 9789811620140

Ghosh S, Khunt N, Webster TJ (2021e) Arsenic removing prokaryotes as potential biofilters. In: Shah M, Couto SR, Biswas JK (eds) An innovative role of biofiltration in waste water treatment plants (WWTPs). Elsevier, pp 65–111. Paperback ISBN: 9780128239469; eBook ISBN: 9780128239476

Ghosh S, Bhattacharya J, Nitnavare R, Webster TJ (2022a) Heavy metal removal by *Bacillus* for sustainable agriculture. In: Islam MT, Rahman M, Pandey P, (eds) *Bacilli* in Agrobiotechnology: plant stress tolerance, bioremediation, and bioprospecting. Springer Nature, Switzerland, pp 1–30. eBook ISBN 978-3-030-85465-2; Print ISBN 978-3-030-85464-5.

Ghosh S, Bhattacharya J, Nitnavare R, Webster TJ (2022b) Microbial remediation of metals by marine bacteria. In: Shah MP, Couto SR (eds) Development in wastewater treatment research and processes: microbial degradation of xenobiotics through bacterial and fungal approach. Elsevier, USA, pp 131–158. ISBN: 978-0-323-85839-7

Ghosh S (2020) Toxic metal removal using microbial nanotechnology. In: Rai M, Golinska P (eds) Microbial nanotechnology. CRC Press, Boca Raton. eBook ISBN: 9780429276330

Ijadpanah-Saravy H, Safari M, Khodadadi-Darban A, Rezaei A (2014) Synthesis of titanium dioxide nanoparticles for photocatalytic degradation of cyanide in wastewater. Anal Lett 47(10):1772–1782

Jamdade DA, Rajpali D, Joshi KA, Kitture R, Kulkarni AS, Shinde VS, Bellare J, Babiya KR, Ghosh S (2019) *Gnidia glauca*-and *Plumbago zeylanica*-mediated synthesis of novel copper nanoparticles as promising antidiabetic agents. Adv Pharmacol Sci 2019:9080279

Karmakar S, Ghosh S, Kumbhakar P (2020) Enhanced sunlight-driven photocatalytic and antibacterial activities of flower-like ZnO@ $MoS_2$ nanocomposite. J Nanopart Res 22:11

Kitture R, Chordiya K, Gaware S, Ghosh S, More PA, Kulkarni P, Chopade BA, Kale SN (2015) ZnO nanoparticles-red sandalwood conjugate: a promising anti-diabetic agent. J Nanosci Nanotechnol 15:4046–4051

Kusworo TD, Kumoro AC, Utomo DP, Kusumah FM, Pratiwi MD (2021) Performance of the crosslinked PVA coated PES-TiO2 nano hybrid membrane for the treatment of pretreated natural rubber wastewater involving sequential adsorption–ozonation processes. J Environ Chem Eng 9:104855

Luikham S, Malve S, Gawali P, Ghosh S (2018) A novel strategy towards agro-waste mediated dye biosorption for water treatment. World J Pharm Res 7(4):197–208

Lv Y, Zhang C, He A, Yang SJ, Wu GP, Darling SB, Xu ZK (2017) Photocatalytic nanofiltration membranes with self-cleaning property for wastewater treatment. Adv Func Mater 27:1700251

Motahari F, Mozdianfard MR, Salavati-Niasari M (2015) Synthesis and adsorption studies of NiO nanoparticles in the presence of $H_2$acacen ligand, for removing Rhodamine B in wastewater treatment. Process Saf Environ Prot 93:282–292

Nataraj SK, Hosamani KM, Aminabhavi TM (2006) Distillery wastewater treatment by the membrane-based nanofiltration and reverse osmosis processes. Water Res 40(12):2349–2356

Qu X, Alvarez PJ, Li Q (2013) Applications of nanotechnology in water and wastewater treatment. Water Res 47:3931–3946

Rajabi HR, Shahrezaei F, Farsi M (2016) Zinc sulfide quantum dots as powerful and efficient nanophotocatalysts for the removal of industrial pollutant. J Mater Sci: Mater Electron 27:9297–9305

Ranpariya B, Salunke G, Karmakar S, Babiya K, Sutar S, Kadoo N, Kumbhakar P, Ghosh S (2021) Antimicrobial synergy of silver-platinum nanohybrids with antibiotics. Front Microbiol 11:610968

Robkhob P, Ghosh S, Bellare J, Jamdade D, Tang IM, Thongmee S (2020) Effect of silver doping on antidiabetic and antioxidant potential of ZnO nanorods. J Trace Elem Med Biol 58:126448

Rokade SS, Joshi KA, Mahajan K, Tomar G, Dubal DS, Singh V, Kitture R, Bellare J, Ghosh S (2017) Novel anticancer platinum and palladium nanoparticles from *Barleria prionitis*. Global J Nanomed 2(5):555600

Rokade S, Joshi K, Mahajan K, Patil S, Tomar G, Dubal DS, Parihar VS, Kitture R, Bellare JR, Ghosh S (2018) *Gloriosa superba* mediated synthesis of platinum and palladium nanoparticles for induction of apoptosis in breast cancer. Bioinorg Chem Appl 2018:4924186

Salunke GR, Ghosh S, Kumar RS, Khade S, Vashisth P, Kale T, Chopade S, Pruthi V, Kundu G, Bellare JR, Chopade BA (2014) Rapid efficient synthesis and characterization of silver, gold, and bimetallic nanoparticles from the medicinal plant *Plumbago zeylanica* and their application in biofilm control. Int J Nanomed 9:2635–2653

Saray AM, Yousefi R, Zare-Dehnavi N, Jamali-Sheini F (2019) Improvement visible-light photocatalytic performance of single-crystalline $SnSe_{1\pm x}$ NPs toward degradation of organic pollutants. Solid State Sci 98:106044

Shende S, Joshi KA, Kulkarni AS, Shinde VS, Parihar VS, Kitture R, Banerjee K, Kamble N, Bellare J, Ghosh S (2017) *Litchi chinensis* peel: a novel source for synthesis of gold and silver nanocatalysts. Global J Nanomed 3(1):555603

Shende S, Joshi KA, Kulkarni AS, Charolkar C, Shinde VS, Parihar VS, Kitture R, Banerjee K, Kamble N, Bellare J, Ghosh S (2018) *Platanus orientalis* leaf mediated rapid synthesis of catalytic gold and silver nanoparticles. J Nanomed Nanotechnol 9:2

Shinde SS, Joshi KA, Patil S, Singh S, Kitture R, Bellare J, Ghosh S (2018) Green synthesis of silver nanoparticles using Gnidia glauca and computational evaluation of synergistic potential with antimicrobial drugs. World J Pharm Res 7(4):156–171

Shirmardi A, Teridi MA, Azimi HR, Basirun WJ, Jamali-Sheini F, Yousefi R (2018) Enhanced photocatalytic performance of ZnSe/PANI nanocomposites for degradation of organic and inorganic pollutants. Appl Surf Sci 462:730–738

Thanuttamavong M, Yamamoto K, Oh JI, Choo KH, Choi SJ (2002) Rejection characteristics of organic and inorganic pollutants by ultra low-pressure nanofiltration of surface water for drinking water treatment. Desalination 145:257–264